frontiers | Frontiers in Earth Science

TYPE Original Research
PUBLISHED 02 February 2023
DOI 10.3389/feart.2023.1128634

OPEN ACCESS

EDITED BY
Danqi Li,
Curtin University, Australia

REVIEWED BY
Li Ma,
Xi'an University of Science and Technology, China
Wenshuai Li,
Shandong University of Science and Technology, China

*CORRESPONDENCE
Yanlong Chen,
chenyanlong@cumt.edu.cn

SPECIALTY SECTION
This article was submitted to Environmental Informatics and Remote Sensing, a section of the journal Frontiers in Earth Science

RECEIVED 21 December 2022
ACCEPTED 23 January 2023
PUBLISHED 02 February 2023

CITATION
Xie Q, Chen Y, Lyu H, Gu J, Chen Y, Cui H and Wu P (2023), Dynamic mechanical properties and energy dissipation analysis of frozen sandstone with initial damage. *Front. Earth Sci.* 11:1128634. doi: 10.3389/feart.2023.1128634

Dynamic mechanical properties and energy dissipation analysis of frozen sandstone with initial damage

Qihang Xie[1], Yanlong Chen[2]*, Haoyan Lyu[1], Jun Gu[1], Yuanguang Chen[1], Huidong Cui[1] and Peng Wu[2]

[1]School of Mechanics and Civil Engineering, China University of Mining and Technology, Xuzhou, China, [2]State Key Laboratory for Geomechanics and Deep Underground Engineering, China University of Mining and Technology, Xuzhou, China

Damaged rock masses on the slopes of open pit coal mines are prone to geological disasters such as landslides under low temperatures and dynamic loads such as blasting impacts. Based on the Low Temperature Split Hopkinson Pressure Bar (LT-SHPB) system, dynamic compressive tests were done on sandstone specimens, which were damaged by uniaxial loading and unloading test. Dynamic stress–strain curves and dynamic mechanical properties of frozen sandstone with initial damage were analyzed as well as the energy dissipation characteristics. The results indicate that both compressive state and plastic deformation state of the dynamic stress-strain curves increase with the increase of the damage value. Dynamic peak stress and dynamic elastic modulus exhibit an evident damage weakening effect while the dynamic peak strain, in contrast, exhibits a damage enhancement effect. In addition, all three dynamic mechanical properties of the damaged frozen sandstone exhibit an impact effect. The dissipation energy ratio and reflection energy ratio of frozen sandstone increase with the increase of initial damage value while the transmission energy ratio decreases. With the increase of initial damage value and strain rate, the energy utilization rate during the sandstone failure process increases, resulting in more small fragments and powders.

KEYWORDS

open pit coal mine, initial damage, LT-SHPB, frozen sandstone, energy dissipation

1 Introduction

Many large open-pit coal mines in China are distributed in the Western cold regions such as Xinjiang (Zhao et al., 2020; Lu et al., 2021). Under the action of low temperature, a special frozen rock slope is formed. Depending on the temperature and moisture content, the freezing expansion of free water in the rock mass brings two effects (Weng et al., 2021): On the one hand, it accelerates the development of damage cracks and weakens the mechanical properties of the rock mass (Ghobadi and Babazadeh, 2015); On the other hand, freezing water fills part of the rock cracks and enhances rock mass strength to some extent (Wang et al., 2019). At present, scholars have made abundant achievements in the study of static mechanical properties of rock at low temperature, mainly in terms of failure strength, elastic modulus, and failure characteristics (Ulrich and Darling, 2001; Feuer and Ince, 2015; Liu X. Y. et al., 2021). In addition, some scholars have studied the triaxial creep properties of frozen rock and obtained the creep equation which can better describe the creep process of the frozen rock (Zhu W. C. et al., 2019; Zhu Z. Y. et al., 2019; Shan et al., 2021).

Open-pit coal mine rocks are generally subjected to loose blasting before stripping, and the external loading mode of the rock by the stress waves generated by blasting is in the form of dynamic impact at a high strain rate (Ding et al., 2019; Shen et al., 2021). Rock mechanical properties under impact load are significantly different from those under static loading (Wang et al., 2016; Zhou et al., 2020). With the increase of geotechnical engineering in cold regions, the research on dynamic mechanical properties of rock under low temperature environments is increasing. Mardoukhi et al. (2021) and Liu C. J. et al. (2021) studied the dynamic tensile properties of granite at low temperature. Weng et al. (2020) compared the dynamic mechanical of dry and saturated Siltstones under sub-zero temperatures, and investigated the mechanism of weakening and strengthening the dynamic mechanical properties of saturated rock samples at sub-zero temperatures by using NMR technology. Yang et al. (2021a; 2021b) found that the dynamic mechanical strength of red sandstone gradually increased from −5°C to −30°C, but decreased sharply when the temperature was below −30°C; Li et al. (2018) investigated the freeze-thaw effect on the pore structure and dynamic mechanical properties of sandstone, and the result shows that sandstone porosity increased with the adding-up of freeze-thaws cycles, which leads to the attenuation of the dynamic mechanical properties of sandstone. Nikolenko et al. (2021) studied the effect of freeze-thaw cycle on the propagation of cracks in coal and found that a large number of cracks formed after a single freeze-thaw cycle. In addition, it has been found by literature review that since the deformation and failure process of rocks is essentially an energy-driven destabilization phenomenon (Xie et al., 2009; Song et al., 2015), the energy analysis method is a convenient and critical perspective to respond to the extent of fracture development within the rock impact damage process (Yang et al., 2020; Wang et al., 2021). For example, Wang et al. (2017) analyzed the energy evolution characteristics of red sandstone during dynamic impact after freeze-thaw cycles and defined Freeze-Thaw-Mechanical coupling damage based on energy dissipation ratio; Weng et al. (2019b) have found that the dynamic fragmentation of dry and saturated siltstones decreased first and then increased from 18°C to −50°C, reaching a minimum value at −30°C while the energy dissipation density of saturated siltstones reached a maximum value at −30°C. Wang et al. (2020) studied the variation law of energy dissipation rate during the impact of frozen sandstone to reflect the strain rate effect and temperature effect of sandstone.

However, previous studies on the dynamic mechanical properties of rock at low temperature mainly focused on intact rock samples, ignoring the influence of initial damage of rock. Defects such as cracks and holes can exist within the rock mass of open pit coal mines. There are two main reasons for the existence of these defects: 1) Geological effects (internal forces such as crustal movement and external forces such as weathering) during the formation of the rock body in nature makes defects of various shapes and sizes appear inside the rock (Cao et al., 2016; Ahmed et al., 2020); 2) The disturbing effect of mining, such as rolling of slope rock mass by large mining trucks and impact of blasting (Hou et al., 2019; Li et al., 2021; Wu et al., 2022). These damages aggravate the deterioration of the mechanical properties of slope rocks and bring about major potential hazards such as landslides. Therefore, it is necessary to analyze the influence of rock damage on the dynamic mechanical properties of rocks.

In this paper, sandstone is chosen as the test object because it is widely present in open-pit coal mine slopes as the main rock layer and its characteristic is representative and applicable (Li et al., 2022). Sandstones with different initial damage were prepared by uniaxial loading and unloading test, and the initial damage value was defined based on the porosity. The real-time low-temperature dynamic compression test was carried out on the damaged sandstone to obtain the variation law of dynamic mechanical parameters of frozen sandstone under different damage conditions. The dynamic damage process of frozen sandstone is analyzed from the perspective of energy, and the energy dissipation characteristics of freeze-damaged sandstone are obtained. The research results can provide a reference for the prevention and control of slope instability during open-pit coal mining in cold regions.

2 Materials and experimental methods

2.1 Preparation of specimen

The sample rock was taken from the area near an open-pit coal mine (Xinjiang, China), which had not been damaged by disturbances such as blasting operations and large mining trucks in the open-pit mine. Judging from the cutting surfaces, the sandstone is in dark red with fine particles and hard texture. The main mineral components of the sandstone are as follows: quartz (61%), muscovite (28%), kaolinite (5%), montmorillonite (3%) as well as small amounts of illite and hematite.

According to the ISRM suggested methods, sandstone was made into Φ50 × 100 mm cylindrical specimens for initial damage treatment. In order to avoid the experimental error caused by the dispersion of sandstone, the longitudinal wave velocity of standard samples was detected. The specimens with similar wave velocities were selected as the test objects, and the basic physical and mechanical parameters of the natural air-dried sandstone specimens are shown in Table 1.

2.2 Initial damage treatment

The initial damage condition of the sandstone specimens was obtained through loading and unloading test using MTS816 electro-hydraulic servo system. According to the uniaxial compressive strength (UCS) σ_c=27.50 MPa of sandstone specimens, four loading stress levels were determined as 0% σ_c, 50% σ_c, 60% σ_c, and 70% σ_c, respectively. When the specimen reached the set stress level during the loading process, the specimen was held for 30 min to ensure that the cracks inside the specimen were fully developed. In this regard, 9 specimens were prepared for each group of damage levels. Finally, three specimens of each group after initial damage treatment were taken for mercury intrusion test to determine the change of porosity, and the remaining six specimens of each group will be used to prepare disk specimens for real-time low temperature SHPB test.

Characterization of damage is the key to defining rock damage and establishing the damage evolution law. In this paper, the initial damage value is defined by the porosity of sandstone specimens. Weng et al. (2019a) proves the validity and feasibility of porosity to evaluate the degree of rock damage. An equation for describing the damage using the porosity is proposed as follows:

TABLE 1 Basic physical and mechanical parameters of sandstone specimens.

Specimen	Density ($g \cdot cm^{-3}$)	Uniaxial compressive strength (MPa)	Elasticity modulus (GPa)	Poisson's ratio	Longitudinal wave velocity ($m \cdot s^{-1}$)
1	2.19	26.17	2.25	0.17	2,624
2	2.34	28.06	2.34	0.18	2,634
3	2.31	28.26	2.38	0.17	2,657
Average	2.28	27.50	2.32	0.17	2,638

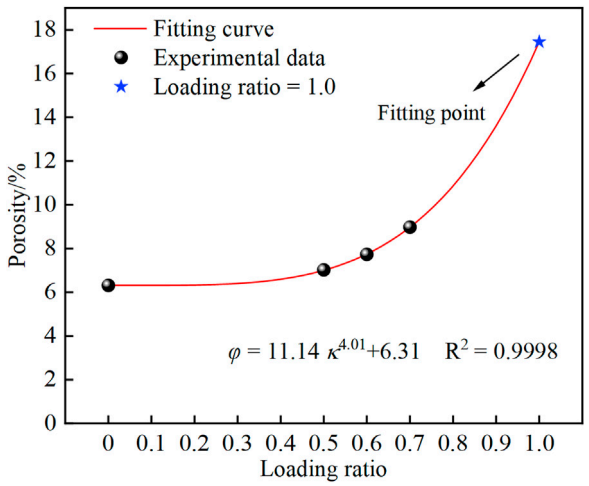

FIGURE 1
Variation of the porosity of sandstone specimens with the loading ratio.

TABLE 2 Initial damage value of sandstone specimen under different loading stress.

Loading stress (MPa)	Loading ratio	φ (%)	D (%)
0	0	6.31	0
13.75	0.50	7.02	6.37
16.50	0.60	7.73	12.75
19.25	0.70	8.98	23.97

$$D = 1 - \frac{\varphi_1 - \varphi}{\varphi_1 - \varphi_0} \quad (1)$$

where, D is the damage value of the rock; φ_0 is the porosity of the undamaged rock; φ_1 is the porosity of the rock at failure; φ is the porosity of the damaged rock. Eq. 1 reflects the overall weakening degree of rock specimen without considering the anisotropy of damage.

Figure 1 shows the variation of the porosity of sandstone specimens with the loading ratio (loading stress over UCS). In fact, the porosity of rock failure is difficult to obtain by experiment. However, the approximation of φ_1 can be obtained by the porosity fitting curve. The fitting equation is as follows:

$$\varphi = 11.14\kappa^{4.01} + 6.31 \quad R^2 = 0.9998 \quad (2)$$

where, κ is the loading ratio. When the loading ratio $\kappa = 1$, we may obtain the approximate porosity of sandstone at failure $\varphi_1 = 17.45\%$. Substituting φ_1 to Eq. 1, the initial damage value under different loading stress can be obtained. Table 2 shows the loading ratio, porosity and initial damage value of sandstone under different loading stresses.

2.3 Real-time low temperature SHPB test

First, four sets of sandstone specimens with different initial damage were processed into disc specimens with 50 mm diameter and 25 mm height. Then, the disc specimens were subjected to natural air-drying treatment in order to eliminate the effects of changes in moisture content during specimen processing and initial damage treatment. Finally, real-time low temperature SHPB test was performed. The test setup and procedure are shown in Figure 2.

Natural air-drying treatment scheme is as follows: first, the sandstone specimens were baked in the oven at 105°C for 24 h; Then, the disk specimens were saturated in a vacuum saturation device for 6 h; Finally, the sandstone specimens were left to dry naturally in an indoor environment for 48 h and then wrapped with plastic wrap and stored in sealed bags. The average moisture content of the natural air-dried sandstone disc specimens is 2.02%.

The LT-SHPB system is used for the real-time low temperature impact test. The test system includes: low-temperature system, launching system, pressure bar system, data collection and processing system, and energy absorption system. Except for the low-temperature system, the composition and functions of the other four systems are the same as those of the conventional SHPB system. The diameter of the compression bar is 50 mm, the density is 7.82 g/cm^3, the longitudinal wave speed is 5,123 m/s, and the modulus of elasticity is 210 GPa. During the test, the low-temperature system provides a real-time low-temperature environment for the sandstone specimen. The temperature control range of low-temperature system is −60°C to room temperature. Cryogenic nitrogen gas is vaporized from liquid nitrogen under the action of electric thermocouple and flows into the cryostat through the hose. When the low-temperature sensor detects that the temperature of the cryostat reaches the preset value, the thermocouple stops working, which is automatically controlled by the low temperature controller. The test shows that the temperature in the cryostat can be stably maintained at the preset temperature with the temperature difference of ±0.2°C.

The temperature of the real-time low-temperature impact test is set at −20°C which is selected based on the average temperature of the sampling mine in winter. It has been found that the sandstone interior needs to be kept freezing for at least 30 min in order to reach the temperature set in the test. In this paper, the temperature holding time

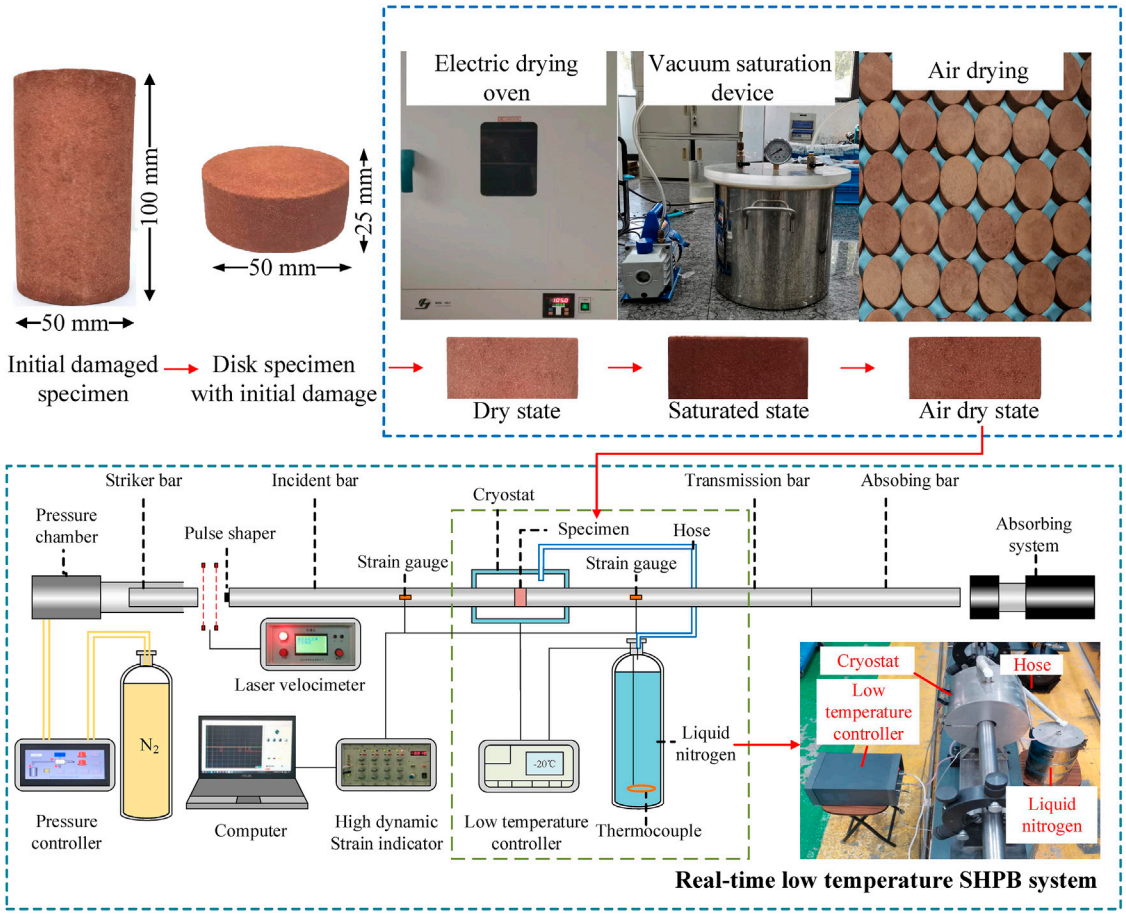

FIGURE 2
Process of real-time low temperature SHPB test.

is set to 1 h for the accuracy of the test data. According to the actual working conditions of blasting in the open pit mine and laboratory equipment conditions, four groups of impact velocity are designed as 3.5, 4.0, 4.5, and 5.0 m/s. The test covered four kinds of initial damage level and four kinds of impact velocity, a total of 16 groups, each group of tests repeated 3 times. And the average strain rates at different impact velocities are 42.1, 76.7, 105.2, and 129.5 s^{-1}, respectively.

3 Results and discussion

3.1 Dynamic stress-strain curve

The dynamic stress-strain curves of frozen sandstone with different initial damage are given in Figures 3A–D. It also shows the dynamic stress-strain curves of damaged sandstone at the strain rate of 76.7 s^{-1} (Figure 3E). Meanwhile, according to the change characteristics of the curve, a typical stress-strain curve for this test is given (Figure 3F), and the typical stress-strain curve is divided into the following four stages:

(I) Compaction stage: This stage is characterized by an upwardly concave curve in appearance. This phenomenon is due to the damage fractures produced in the initial damage treatment process. During the initial loading phase of the sandstone specimen, the fractures are gradually compacted and closed, and plastic deformation is produced.

(II) Elastic deformation stage: This stage manifests itself in appearance as a nearly straight line. The cracks inside the sandstone specimen tend to a stable state after the compaction stage, and no new cracks are generated. As the load continues to increase, the specimen begins to store a large amount of strain energy and will only release a small amount of energy. Since the slope of the curve at this stage is approximately constant, the slope of the curve at this stage is taken as the dynamic elastic modulus in this paper.

(III) Plastic deformation stage: The form of this stage shows a downward concave curve. After the elastic phase, the sandstone specimen develops new cracks as the load continues to increase. The old and new cracks will enter a non-stable extension phase and will gradually penetrate releasing a large amount of energy which will cause increased deformation and even local failure.

(IV) Failure stage: In this stage, the stress of sandstone decreases rapidly in a nearly linear form with the increase of strain. As the sandstone specimen is in the unloading stage, the specimen has been detached from the incident and transmission bar.

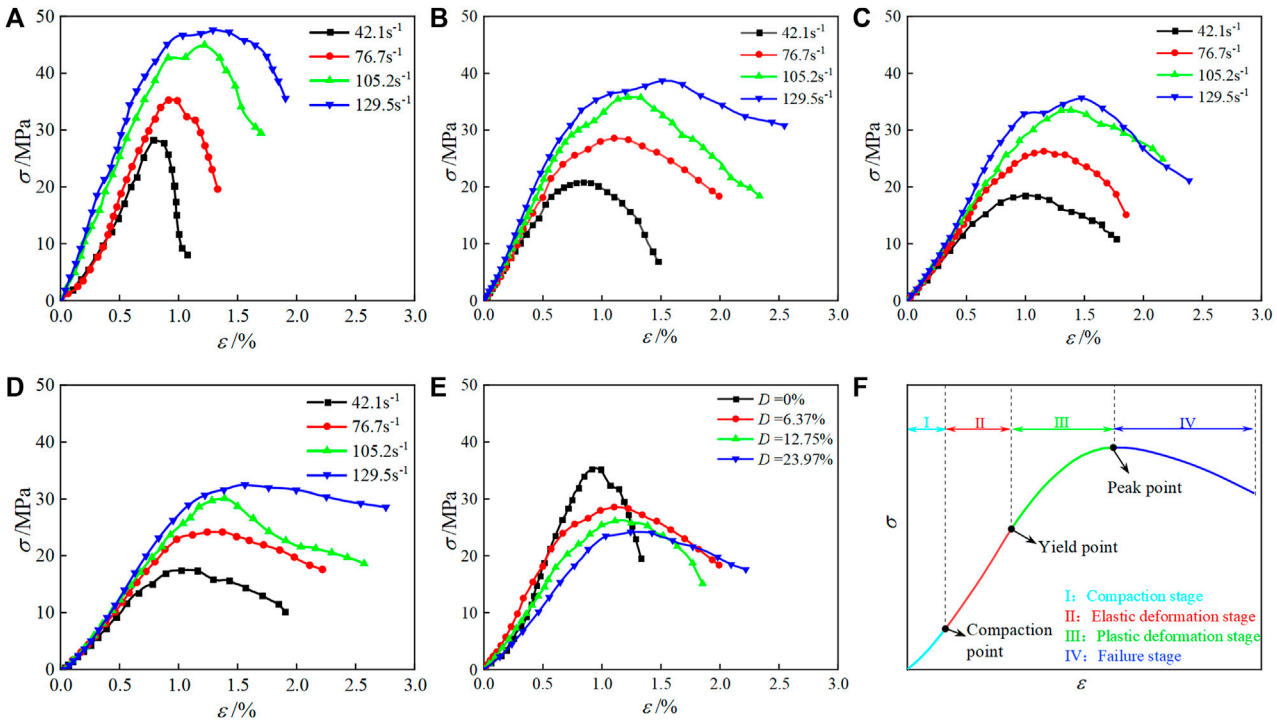

FIGURE 3
Dynamic stress-strain curves of frozen sandstone with initial damage: **(A)** D=0%; **(B)** D=6.37%; **(C)** D=12.75%; **(D)** D=23.97%; **(E)** $\dot{\varepsilon}$ =76.7s^{-1}; **(F)** Typical curve.

TABLE 3 Dynamic mechanical parameters of frozen sandstone under different conditions.

D (%)	$\dot{\varepsilon}$ (s^{-1})	σ_c (MPa)	ε_c (%)	E_c (GPa)
0	42.1	28.63	0.82	4.43
	76.7	35.42	0.95	4.68
	105.2	44.82	1.18	5.80
	129.5	47.64	1.36	6.12
6.37	42.1	20.88	0.84	3.38
	76.7	28.58	1.10	4.14
	105.2	35.80	1.28	4.32
	129.5	38.70	1.51	4.81
12.75	42.1	19.50	0.95	2.57
	76.7	26.28	1.20	3.02
	105.2	33.54	1.35	3.12
	129.5	35.21	1.54	3.86
23.97	42.1	17.52	1.07	2.51
	76.7	24.20	1.28	2.82
	105.2	30.27	1.40	2.85
	129.5	32.50	1.60	3.34

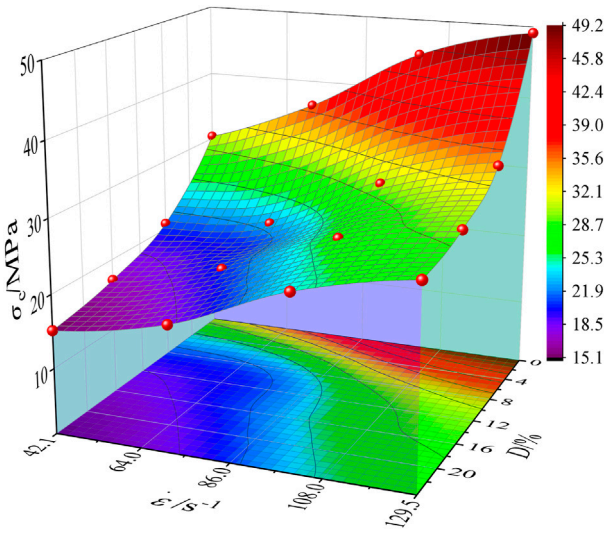

FIGURE 4
Coupling effect of initial damage and strain rate on dynamic peak stress.

As can be seen from Figures 3A–E, the shapes of the curves are basically the same, but there are differences in their trends. Under a certain strain rate, the compaction stage increases with the increase of

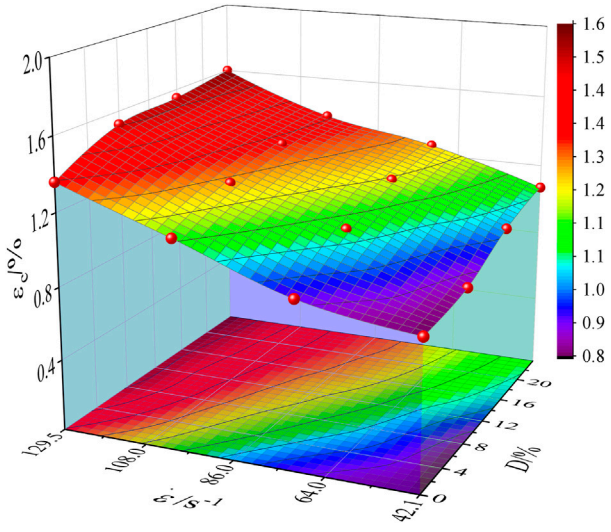

FIGURE 5
Coupling effect of initial damage and strain rate on dynamic peak strain.

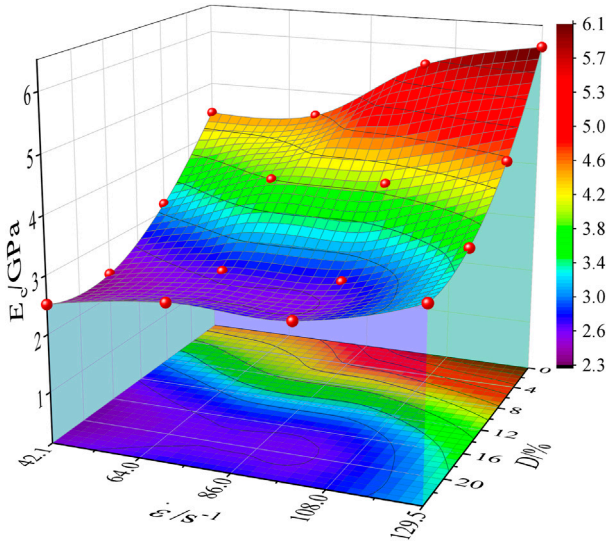

FIGURE 6
Coupling effect of initial damage and strain rate on dynamic elasticity modulus.

damage value. This is because with the increase of damage value, there will be more micro defects in the sandstone sample. In the initial stage of impact loading, defects will gradually close with the increase of load, resulting in a longer compaction stage of the curve. At the same time, with the increase of initial damage, the plastic deformation stage also shows an obvious increasing feature.

3.2 Dynamic compressive mechanical parameters of sandstone

Dynamic mechanical parameters of frozen sandstone at different strain rates and different initial damage values, including dynamic peak stress, dynamic peak strain and dynamic elastic modulus, were obtained from the dynamic stress-strain curves (Table 3).

3.2.1 Dynamic peak stress

Figure 4 shows the variation surface of dynamic peak stress of frozen sandstone under the coupling effect of initial damage and strain rate. As can be seen from the figure, the initial damage value and strain rate significantly affect the dynamic peak stress of the frozen sandstone.

The dynamic peak stress in the frozen sandstone decreases as the initial damage value increases, showing a significant damage weakening effect. Specifically, as the initial damage increased from 0 to 23.97% under four sets of strain rate, the dynamic peak stress of the frozen sandstone decreased from 28.63, 35.42, 44.82, and 47.64 MPa to 17.52, 24.20, 30.27, and 32.50 MPa with a reduction of 38.81%, 31.68%, 32.46%, and 31.78%, respectively. This is due to the increase of damage value, more crack defects appear in the frozen sandstone, which reducing the bearing capacity of frozen sandstone.

For the same condition of initial damage value, the dynamic peak stress of frozen sandstone increases with increasing strain rate, showing a significant strain rate strengthening effect. Under the four sets of damage values, with the increase of strain rate, the dynamic peak stress of frozen sandstone increased from 28.63, 20.88, 19.50, and 17.52 MPa to 47.64, 38.70, 35.21, and 32.50 MPa, which increased by 66.40%, 85.34%, 80.56%, and 85.50%, respectively.

3.2.2 Dynamic peak strain

Figure 5 shows the variation surface of dynamic peak strain of frozen sandstone under the coupling effect of initial damage and strain rate. Contrary to the dynamic peak stress, the dynamic peak strain of frozen sandstone increases with the increase of damage value, showing a damage strengthening effect. As the initial damage increased from 0 to 23.97% under four sets of strain rate, the dynamic peak strain decreased from 0.82%, 0.95%, 1.18%, and 1.36% to 1.07%, 1.28%, 1.40%, and 1.60% with an increase of 30.49%, 34.74%, 18.64%, and 17.65%, respectively. Due to the presence of initial damage, cracks and defects within the sandstone increase, causing a tendency of plasticity enhancement.

With the increase of strain rate, the peak strain increases linearly and rapidly, showing a strain rate strengthening effect. The dynamic peak strain of the frozen sandstone increases from 0.82%, 0.84%, 0.95%, and 1.07% to 1.36%, 1.51%, 1.54%, and 1.60% with an increase of 65.85%, 79.76%, 62.11%, and 49.53% respectively when the strain rate increases from 42.1 s^{-1} to 129.5 s^{-1} for the four sets of initial damage conditions.

3.2.3 Dynamic elastic modulus

As can be seen from the Figure 6, the variation characteristics of dynamic elastic modulus of the frozen sandstone are basically consistent with the dynamic peak stress. When the initial damage increases from 0 to 23.97% under the conditions of four groups of strain rates, the dynamic elastic modulus decreases from 4.43, 4.68, 5.80, and 6.12 GPa to 2.51, 2.82, 2.85, and 3.34 GPa, respectively, which decreases by 43.34%, 39.74%, 50.86%, and 45.42%, showing obvious damage weakening characteristics. In addition, under the four

groups of initial damage, with the increase of strain rate, the dynamic elastic modulus increases from 4.43, 3.38, 2.57, and 2.51 GPa to 6.12, 4.81, 3.86, and 3.34 GPa, respectively, which increased by 38.15%, 42.31%, 50.19%, and 33.07%, showing a strain rate strengthening effect.

3.3 Energy dissipation characteristics

The failure of sandstone samples under external load will experience the propagation and growth of defects such as internal cracks and holes until these defects penetrate the whole sample and make it completely destroyed. All these processes involve the absorption, transformation and dissipation of energy. It can be seen that the analysis of the dynamic damage process of frozen sandstone from an energy perspective can effectively reveal the damage effect and impact effect of frozen sandstone in the process of dynamic failure.

3.3.1 Energy calculation

The failure process of sandstone specimens under dynamic loading is accompanied by the variation in energy. The incident energy W_I input to the sandstone specimen from the impact bar is converted into three components, namely the transmitted energy W_T entering the transmission bar, the reflected energy W_R reflected back into the incident bar and the dissipated energy W_D used to destroy the sandstone specimen. The relationship between these four components of energy can be expressed in Eq. 3:

$$W_D = W_I - W_R - W_T \tag{3}$$

According to classical elastic pressure bar theory, the incident energy W_I, reflected energy W_R, transmitted energy W_T, and dissipated energy W_D in the above equation can all be calculated by the equation, which is expressed as:

$$\begin{cases} W_I(t) = E_S C_S A_S \int_0^t \varepsilon_I^2(t)\mathrm{d}t \\ W_R(t) = E_S C_S A_S \int_0^t \varepsilon_R^2(t)\mathrm{d}t \\ W_T(t) = E_S C_S A_S \int_0^t \varepsilon_T^2(t)\mathrm{d}t \end{cases} \tag{4}$$

where E_S, C_S and A_S are the elastic modulus, stress wave propagation velocity and cross-sectional area of the pressure bar in the SHPB system.

R_R, R_T and R_D represent the ratios of reflected energy W_R, transmitted energy W_T and dissipated energy W_D to their incident energy W_I, respectively, as calculated in Eq. 5:

$$\begin{cases} R_R = W_R/W_I \\ R_T = W_T/W_I \\ R_D = W_D/W_I \end{cases} \tag{5}$$

The dissipated energy in the SHPB dynamic compression test is mainly used for the expansion and penetration of defects such as cracks and holes within the sandstone specimen, but is also accompanied by kinetic energy and other forms of energy carried by the broken rock mass during the destruction of the specimen, such as heat energy and acoustic energy. However, 95% of the dissipated energy is mainly used for the expansion and penetration of defects, with a small proportion of the remaining 5% being used for other forms of energy (Zhang et al., 2000). Therefore, this 5% of other forms of energy will be ignored in this study and the dissipated energy will be considered directly as the fracture energy of the sandstone specimen during dynamic compression failure.

Through Eqs 3–5, the calculation results of W_I, W_R, W_T, and W_D of damaged sandstone under different initial damage values and strain rates in the real-time low-temperature dynamic compression failure process and the ratio of each energy to the incident energy W_I are obtained. The specific results are shown in Table 4.

3.3.2 Effect of initial damage value and strain rate on the energy dissipation characteristic

Figure 7 shows the histogram of the variation of incident energy, reflected energy, transmitted energy, and dissipated energy with damage values and the impact failure morphology of the damaged sandstone, which helps to analyze the change of sandstone failure characteristics in the process of dynamic compression from the aspect of energy change.

As can be seen from Figure 7, the incident, reflected, transmitted and dissipated energies all increase with increasing strain rate. For the same strain rate, the incident energy of the damaged frozen sandstone remains in a relatively constant state, and basically does not change with the change of damage value. This is due to the fact that the incident energy is related to the impact velocity. And the strain rate is almost corresponding to the impact velocity. When the impact velocity is relatively constant, the incident energy of the rod is also relatively constant, which reflects the stability of the LT-SHPB system. In addition, with the increase of damage value, the reflected energy and dissipated energy increase, while the transmitted energy decreases. In terms of sandstone failure morphology, the frozen sandstone will failure in a higher degree of fragmentation with more powder particles. The increased damage value also increases the degree of impact damage to the frozen sandstone, resulting in more and smaller fragments. This is due to the fact that as the damage value increases, the cracks and fissures within the frozen sandstone increase significantly, its structural integrity decreases obviously. Based on the basic morphology of fragments, it can be judged that the failure of frozen sandstone is mainly transformed from tensile failure mode to composite failure mode with the increase of strain rate and initial damage.

Figure 8 shows the variation curves of the reflected energy ratio R_R, transmitted energy ratio R_T and dissipated energy ratio R_D with damage values for different strain rates. The reflected energy ratio increases gradually with increasing damage values, which corresponds to the increase in dynamic peak strain in frozen sandstone with increasing damage values. Moreover, the transmitted energy ratio and dissipated energy ratio of the damaged frozen sandstone at the four sets of strain rates show a clear damage effect. The transmitted energy ratio decreases as the damage value increases while the dissipated energy ratio increases. In other words, the energy utilization rate during sandstone failure process increases with the increase of damage value. It shows that with the increase of damage value in dynamic failure of damaged frozen sandstone, more energy is consumed for the propagation of internal cracks and holes. This is consistent with the phenomenon that more block debris and granular

10.3389/feart.2023.1128634

TABLE 4 The energy value during dynamic failure of damaged frozen sandstone.

$\dot{\varepsilon}$ (s^{-1})	D (%)	W_I (J)	W_R (J)	R_R (%)	W_T (J)	R_T (%)	W_D (J)	R_D (%)
42.1	0	44.56	21.68	48.65	16.91	37.95	5.97	13.40
	6.37	48.17	23.00	47.75	17.46	36.25	7.71	16.01
	12.75	45.14	23.78	52.68	13.13	29.09	8.23	18.23
	23.97	46.65	25.26	54.15	12.02	25.77	9.37	20.09
76.7	0	74.99	38.73	51.65	23.85	31.80	12.41	16.55
	6.37	76.99	40.35	52.41	20.08	26.08	16.56	21.51
	12.75	76.86	42.02	54.67	16.36	21.29	18.48	24.04
	23.97	78.90	42.54	53.92	17.05	21.61	19.31	24.47
105.2	0	110.83	59.91	54.06	26.67	24.06	24.25	21.88
	6.37	113.10	62.50	55.26	21.09	18.65	29.51	26.09
	12.75	114.05	61.17	53.63	22.12	19.40	30.76	26.97
	23.97	111.40	63.74	57.22	16.91	15.18	30.75	27.60
129.5	0	140.12	80.40	57.38	30.08	21.47	29.64	21.15
	6.37	143.31	82.89	57.84	26.46	18.46	33.96	23.70
	12.75	141.55	84.58	59.75	21.78	15.39	35.19	24.86
	23.97	138.76	85.44	61.57	15.67	11.29	37.65	27.13

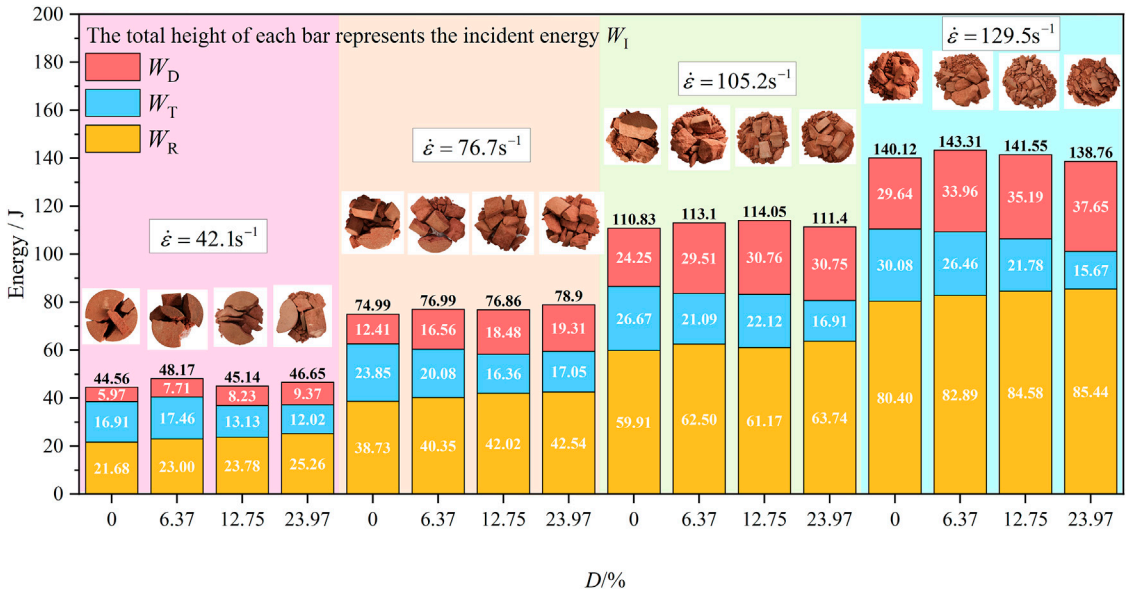

FIGURE 7
Energy variation and failure morphology of frozen sandstone with different initial damage values and strain rates.

powder will appear with the increase of damage value in the dynamic failure process of sandstone. In addition, as the strain rate increases, the dissipated energy ratio gradually increases, and the energy utilization rate in the process of sandstone failure increases, which is similar to the influence of the initial damage value on the dissipated energy ratio. The strain rate can effectively improve the energy utilization rate during sandstone failure process and reduce the proportion of energy lost due to transmission.

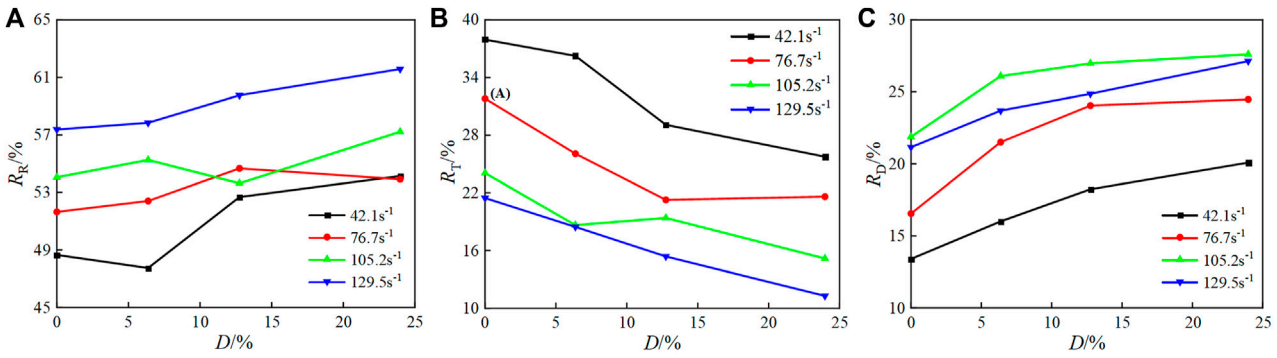

FIGURE 8
Energy ratio variation curves of frozen sandstone with different initial damage values **(A)** Reflected energy ratio; **(B)** Transmitted energy ratio; **(C)** Dissipated energy ratio.

4 Conclusion

This paper aims to investigate the effect of initial damage on dynamic mechanical response of the frozen sandstone. The dynamic compression test of frozen sandstone under different initial damage was carried out by LT-SHPB test system. Based on the theory of energy dissipation, the dynamic mechanical properties and the energy dissipation law were studied. The main conclusions are as follows:

(1) The stress-strain curve of the damaged frozen sandstone can be divided into four stages: compaction stage, elastic deformation stage, plastic deformation stage, and failure stage. The compression stage and plastic deformation stage of the frozen sandstone increase with the increasing initial damage value at the same strain rate.
(2) Initial damage has a significant effect on the dynamic mechanical response of frozen sandstone. The dynamic peak stress and dynamic elastic modulus of frozen sandstone decrease with the increase of the initial damage value, showing an obvious damage weakening effect. Dynamic peak strains, in contrast, increase with the increasing damage value. In addition, the dynamic peak stress, dynamic elastic modulus and dynamic peak strain all exhibit a strain rate effect that increase with the increase of strain rate.
(3) As the strain rate and initial damage value increase, the frozen sandstone will failure in a higher degree of fragmentation with more powder particles. The failure of frozen sandstone is mainly transformed from tensile failure to composite failure with the increase of strain rate and initial damage value.
(4) Under the same strain rate, the incident energy of damaged frozen sandstone can remain in a relatively stable state. The reflected energy ratio and dissipated energy ratio increase with the increasing initial damage value, while the transmitted energy ratio reduces. As initial damage value and strain rate increase, the energy utilization rate increases, which is consistent with the phenomenon that more small fragments and granular powders appear during the dynamic failure process of the frozen sandstone.

Data availability statement

The original contributions presented in the study are included in the article/Supplementary Material, further inquiries can be directed to the corresponding author.

Author contributions

QX and YaC designed the study and wrote the manuscript. QX, HL, JG, YuC, and HC obtained and analyzed data for the research. QX, HC, and PW prepared the figures. All authors contributed to the discussion of research results and manuscript revision.

Funding

This work was financially supported by the National Key R&D Program of China (2022YFC2903902) and the National Natural Science Foundation of China (51974295).

Acknowledgments

The authors thank State Key Laboratory for Geomechanics and Deep Underground Engineering for providing experimental equipment. It is also grateful for the financial support provided by the National Key R&D Program of China and the National Natural Science Foundation of China.

Conflict of interest

The authors declare that the research was conducted in the absence of any commercial or financial relationships that could be construed as a potential conflict of interest.

Publisher's note

References

Ahmed, Z., Wang, S. H., Hashmi, M. Z., Zhang, Z. S., and Zhu, C. J. (2020). Causes, characterization, damage models, and constitutive modes for rock damage analysis: A review. *Arabian J. Geosciences* 13 (16), 806. doi:10.1007/s12517-020-05755-3

Cao, R. H., Cao, P., Lin, H., Pu, C. Z., and Ou, K. (2016). Mechanical behavior of brittle rock-like specimens with pre-existing fissures under uniaxial loading: Experimental studies and particle mechanics approach. *Rock Mech. Rock Eng.* 49 (3), 763–783. doi:10.1007/s00603-015-0779-x

Ding, X. H., Zhou, W., Lu, X., Li, M., Manda, E., Shi, X. Y., et al. (2019). Distribution characteristics of fragments size and optimization of blasting parameters under blasting impact load in open-pit mine. *Ieee Access* 7, 137501–137516. doi:10.1109/Access.2019.2942968

Feuer, M., and Ince, I. (2015). Effects of the freeze-thaw (F-T) cycle on the andesitic rocks (Sille-Konya/Turkey) used in construction building. *J. Afr. Earth Sci.* 109, 96–106. doi:10.1016/j.jafrearsci.2015.05.006

Ghobadi, M. H., and Babazadeh, R. (2015). Experimental studies on the effects of cyclic freezing-thawing, salt crystallization, and thermal shock on the physical and mechanical characteristics of selected sandstones. *Rock Mech. Rock Eng.* 48 (3), 1001–1016. doi:10.1007/s00603-014-0609-6

Hou, R. B., Zhang, K., Tao, J., Xue, X. R., and Chen, Y. L. (2019). A nonlinear creep damage coupled model for rock considering the effect of initial damage. *Rock Mech. Rock Eng.* 52 (5), 1275–1285. doi:10.1007/s00603-018-1626-7

Li, J. L., Kaunda, R. B., and Zhou, K. P. (2018). Experimental investigations on the effects of ambient freeze-thaw cycling on dynamic properties and rock pore structure deterioration of sandstone. *Cold Regions Sci. Technol.* 154, 133–141. doi:10.1016/j.coldregions.2018.06.015

Li, X., Li, Q., Hu, Y., Teng, L., and Yang, S. (2021). Evolution characteristics of mining fissures in overlying strata of stope after converting from open-pit to underground. *Arabian J. Geosciences* 14 (24), 2795. doi:10.1007/s12517-021-08978-0

Li, X., Peng, J., Xie, Y., Li, Q., Zhou, T., Wang, J., et al. (2022). Influence of high-temperature treatment on strength and failure behaviors of a quartz-rich sandstone under true triaxial condition. *Lithosphere* 2022 (10). doi:10.2113/2022/3086647

Liu, C. J., Wang, D. G., Wang, Z. X., Ke, B., Li, P., and Yu, S. T. (2021a). Dynamic splitting tensile test of granite under freeze-thaw weathering. *Soil Dyn. Earthq. Eng.* 140, 106411. doi:10.1016/j.soildyn.2020.106411

Liu, X. Y., Liu, L. L., Li, Z., and Yao, Z. M. (2021b). Experimental analysis on creep properties of frozen silty mudstone considering conservation of energy. *J. Test. Eval.* 49 (1), 417–434. doi:10.1520/Jte20180707

Lu, X., Zhou, W., Cai, Q., Li, M., Luan, B., and Liu, F. (2021). Mechanical properties and meso fracture mechanism of mudstone under freeze-thaw cycle. *J. Min. Saf. Eng.* 38 (04), 819–829. doi:10.13545/j.cnki.jmse.2020.0633

Mardoukhi, A., Mardoukhi, Y., Hokka, M., and Kuokkala, V. T. (2021). Effects of test temperature and low temperature thermal cycling on the dynamic tensile strength of granitic rocks. *Rock Mech. Rock Eng.* 54 (1), 443–454. doi:10.1007/s00603-020-02253-6

Nikolenko, P. V., Epshtein, S. A., Shkuratnik, V. L., and Anufrenkova, P. S. (2021). Experimental study of coal fracture dynamics under the influence of cyclic freezing–thawing using shear elastic waves. *Int. J. Coal Sci. Technol.* 8 (4), 562–574. doi:10.1007/s40789-020-00352-x

Shan, R. L., Bai, Y., Ju, Y., Han, T. Y., Dou, H. Y., and Li, Z. L. (2021). Study on the triaxial unloading creep mechanical properties and damage constitutive model of red sandstone containing a single ice-filled flaw. *Rock Mech. Rock Eng.* 54 (2), 833–855. doi:10.1007/s00603-020-02274-1

Shen, W. L., Shi, G. C., Wang, Y. G., Bai, J. B. A., Zhang, R. F., and Wang, X. Y. (2021). Tomography of the dynamic stress coefficient for stress wave prediction in sedimentary rock layer under the mining additional stress. *Int. J. Min. Sci. Technol.* 31 (4), 653–663. doi:10.1016/j.ijmst.2021.04.003

Song, D., Wang, E., Li, Z., Liu, J., and Xu, W. (2015). Energy dissipation of coal and rock during damage and failure process based on EMR. *Int. J. Min. Sci. Technol.* 25 (05), 787–795. doi:10.1016/j.ijmst.2015.07.014

Ulrich, T. J., and Darling, T. W. (2001). Observation of anomalous elastic behavior in rock at low temperatures. *Geophys. Res. Lett.* 28(11), 2293–2296. doi:10.1029/2000gl012480

Wang, C., Li, S., Zhang, T., and You, Z. (2019). Experimental study on mechanical characteristics and fracture patterns of unfrozen/freezing saturated coal and sandstone. *Materials* 12 (6), 992. doi:10.3390/ma12060992

Wang, F., Wang, H. B., Xu, Y., Cheng, B., and Wang, Q. Q. (2021). Analysis of energy dissipation characteristics of damaged sandstone under impact load. *Shock Vib.* 2021, 1–10. doi:10.1155/2021/4200452

Wang, L., Qin, Y., Jia, H. B., Su, H. M., and Chen, S. G. (2020). Study on mechanical properties and energy dissipation of frozen sandstone under shock loading. *Shock Vib.* 2020, 1–12. doi:10.1155/2020/8893128

Wang, P., Xu, J. Y., Fang, X. Y., and Wang, P. X. (2017). Energy dissipation and damage evolution analyses for the dynamic compression failure process of red-sandstone after freeze-thaw cycles. *Eng. Geol.* 221, 104–113. doi:10.1016/j.enggeo.2017.02.025

Wang, P., Xu, J. Y., Liu, S., Wang, H. Y., and Liu, S. H. (2016). Static and dynamic mechanical properties of sedimentary rock after freeze-thaw or thermal shock weathering. *Eng. Geol.* 210, 148–157. doi:10.1016/j.enggeo.2016.06.017

Weng, L., Wu, Z. J., Liu, Q. S., Chu, Z. F., and Zhang, S. L. (2021). Evolutions of the unfrozen water content of saturated sandstones during freezing process and the freeze-induced damage characteristics. *Int. J. Rock Mech. Min. Sci.* 142, 104757. doi:10.1016/j.ijrmms.2021.104757

Weng, L., Wu, Z. J., and Liu, Q. S. (2020). Dynamic mechanical properties of dry and water-saturated siltstones under sub-zero temperatures. *Rock Mech. Rock Eng.* 53 (10), 4381–4401. doi:10.1007/s00603-019-02039-5

Weng, L., Wu, Z. J., and Liu, Q. S. (2019a). Evaluating damage and microcracking behavior of granite using NMR testing under different levels of unconfined compression. *Int. J. Geomechanics* 19 (1). doi:10.1061/(Asce)Gm.1943-5622.0001335

Weng, L., Wu, Z. J., Liu, Q. S., and Wang, Z. Y. (2019b). Energy dissipation and dynamic fragmentation of dry and water-saturated siltstones under sub-zero temperatures. *Eng. Fract. Mech.* 220, 106659. doi:10.1016/j.engfracmech.2019.106659

Wu, H., Chen, Y., Lv, H., Xie, Q., Chen, Y., and Gu, J. (2022). Stability analysis of rib pillars in highwall mining under dynamic and static loads in open-pit coal mine. *Int. J. Coal Sci. Technol.* 9 (1), 38. doi:10.1007/s40789-022-00504-1

Xie, H., Li, L., Peng, R., and Ju, Y. (2009). Energy analysis and criteria for structural failure of rocks. *J. Rock Mech. Geotechnical Eng.* 1 (01), 11–20. doi:10.3724/sp.j.1235.2009.00011

Yang, R. S., Li, W. Y., and Yue, Z. W. (2020). Comparative study on dynamic mechanical properties and energy dissipation of rocks under impact loads. *Shock Vib.* 2020, 1–15. doi:10.1155/2020/8865099

Yang, Y., Zhang, N. N., and Wang, J. G. (2021b). A study on the dynamic strength deterioration mechanism of frozen red sandstone at low temperatures. *Minerals* 11 (12), 1300. doi:10.3390/min11121300

Yang, Y., Zhang, N. N., and Wang, J. G. (2021a). Fracture morphology analysis of frozen red sandstone under impact. *Shock Vib.* 2021, 1–12. doi:10.1155/2021/4388132

Zhang, Z. X., Kou, S. Q., Jiang, L. G., and Lindqvist, P. A. (2000). Effects of loading rate on rock fracture: Fracture characteristics and energy partitioning. *Int. J. Rock Mech. Min. Sci.* 37(5), 745–762. doi:10.1016/S1365-1609(00)00008-3

Zhao, H., Tian, Y., Guo, Q., Li, M., and Wu, J. (2020). The slope creep law for a soft rock in an open-pit mine in the Gobi region of Xinjiang, China. *Int. J. Coal Sci. Technol.* 7 (2), 371–379. doi:10.1007/s40789-020-00305-4

Zhou, L., Niu, C. Y., Zhu, Z. M., Ying, P., Dong, Y. Q., and Deng, S. (2020). Fracture properties and tensile strength of three typical sandstone materials under static and impact loads. *Geomechanics Eng.* 23 (5), 467–480. doi:10.12989/gae.2020.23.5.467

Zhu, W. C., Li, S. H., Li, S., and Niu, L. L. (2019a). Influence of dynamic disturbance on the creep of sandstone: An experimental study. *Rock Mech. Rock Eng.* 52 (4), 1023–1039. doi:10.1007/s00603-018-1642-7

Zhu, Z. Y., Luo, F., Zhang, Y. Z., Zhang, D. J., and He, J. L. (2019b). A creep model for frozen sand of Qinghai-Tibet based on Nishihara model. *Cold Regions Sci. Technol.* 167, 102843. doi:10.1016/j.coldregions.2019.102843